Energy efficiency maximization for active RIS-aided integrated sensing and communication

Mohamed Rihan[1,4]*, Alessio Zappone[2], Stefano Buzzi[2,3], Dirk Wübben[1] and Armin Dekorsy[1]

*Correspondence:
elmeligy@ant.uni-bremen.de

[1] Department
of Communications Engineering,
University of Bremen,
28359 Bremen, Germany
[2] Department of Electrical
and Information Engineering
(DIEI), University of Cassino
and Southern Lazio,
03043 Cassino, Italy
[3] Dipartimento di Elettronica,
Informazione e Bioingegneria
(DEIB), Politecnico di Milano,
20133 Milan, Italy
[4] Department of Electronics
and Electrical Communications
Engineering, Faculty of Electronic
Engineering, Menoufia
University, Menouf 32952, Egypt

Abstract

This paper investigates energy-efficient communication within an integrated sensing and communication system. The system employs a dual-function radar-communication base station. This base station concurrently serves multiple mobile users for communication purposes while also performing target sensing within a designated range cell. An active reconfigurable intelligent surface (RIS) is utilized to enhance communication efficiency. The focus of this work is to optimize the communication energy efficiency by jointly allocating the transmit power and configuring the RIS elements. This optimization is achieved while satisfying constraints on both the probing power required for target sensing and the quality-of-service demands of the communication users. Two novel optimization methods are proposed, combining techniques from alternating optimization, sequential programming, and fractional programming. Through numerical simulations, the effectiveness of the developed algorithms is validated. Additionally, the performance of the system utilizing an active RIS is compared to that of a system with a passive RIS, specifically in terms of their respective communication energy efficiencies.

Keywords: Integrated sensing and communications (ISAC), Reconfigurable intelligent surface (RIS), Energy efficiency (EE)

1 Introduction

Future-generation wireless networks are expecting a skyrocketing increase in their needs to support both high spectral efficiency and massive connectivity in addition to high-precision sensing through integrating sensing and communication systems into a unique platform, which consequently poses higher energy consumption requirements [1]. Accordingly, the energy efficiency (EE), defined as the ratio of spectral efficiency in (bits/sec/Hz) over the system consumed power in (Watt), has been emerged as a new prominent performance metric for designing sustainable and green wireless networks with integrated sensing and communication (ISAC) capabilities [2, 3]. Then, no wonder to see such convergence and interest from both academia and industry, to study how the enabling technologies for future 6 G networks can help in developing perceptive, sensing-enabled networks with enhanced EE [4, 5].

EE for future 6 G networks is a key requirement for some of the 17 United Nations Sustainable Development Goals, e.g., Goal 9 (Industry, innovation, and Infrastructure), Goal 11 (Sustainable Cities and Communities), and Goal 13 (Climate Action) [1]. On the other hand, the increasing demand for wireless data services has led to the proliferation and densification of wireless infrastructures, which calls for EE in order to reduce OPEX for telecommunication operators. This paper focuses on the communication energy-efficient design of a wireless system incorporating two of the principal innovations brought by 6 G systems, i.e., ISAC [2, 6], and reconfigurable intelligent surfaces (RISs) [4, 7]. Indeed, the impressive progress of MIMO technologies has been an enabler for the realization of both sensing and communication tasks through shared transceivers and RF components [6]; similarly, progress in meta-material technologies has made it possible to introduce in the design of future wireless systems RISs, with the aim of tuning the propagation environment for increased performance and efficiency [7–9]. Researchers have developed energy-efficient designs for RIS-aided downlink multi-user MISO systems, with no sensing capabilities, and developed energy-efficient designs for both the transmit power allocation and the RIS passive beamforming for RIS-aided downlink multi-user MISO system, under maximum power and individual quality of service (QoS) constraints for the users [4]. Additionally, the use of RISs for radar sensing purposes only has also been investigated in the recent past [10, 11]. The paper [12] is one of the first that considers a RIS-aided ISAC scenario; here, however, a passive RIS is considered and the optimized performance metric is not the EE.

On a parallel theme, RIS has recently presented as one of the principal drivers of 6 G wireless networks due to its ability to synthesize the propagation environment in such a way that enables the network to improve its performance merits [3, 13–15]. In other words, RISs are revolutionizing wireless communication by acting as intelligent walls consisting of a large number of reflecting elements that have the ability to manipulate radio waves through changing the phase shifts and/or signal amplitude of the reflected signals from these reflecting elements [16]. This technology offers a plethora of benefits, including enhanced signal coverage and quality, particularly in challenging environments. RIS also improves network capacity by directing signals toward specific users, reducing interference and maximizing the use of the limited radio spectrum [17]. Furthermore, unlike static BSs, RIS can dynamically adjust its configuration in real time, enabling targeted beamforming and improving user experience and system efficiency. Finally, by optimizing signal propagation, RIS contributes to a more sustainable network by reducing the energy consumption needed for BSs to reach users. Overall, RIS holds immense potential to transform wireless communication by offering improved coverage, capacity, and efficiency, paving the way for a more robust and flexible future for wireless networks [17]. Recently, RISs have been also employed to enhance the outage performance of NOMA-based cognitive non-terrestrial network, which has been considered by many researchers and key technological players as the promising architecture for future 6 G networks [18, 19]. Also, RISs have been leveraged to the enhance the performance of the satellite-terrestrial relay network and secrecy performance of internet of things network (IoT) [20, 21]. The contributions presented in papers [22, 23] offer comprehensive insights into various aspects of RIS-assisted communication systems. Beginning with [22], the

Rihan *et al. J Wireless Com Network*   (2024) 2024:20

Page 3 of 22

investigation delves into covert communications within an active RIS-aided multiple-input single-output non-orthogonal multiple access (NOMA) framework, proposing an alternative optimization algorithm to maximize covert rates effectively. Building upon this, [24] discusses the co-optimized performance of multi-RIS-assisted integrated satellite-unmanned aerial vehicle-terrestrial networks (IS-UAV-TNs), emphasizing the installation of RIS on UAVs to reshape wireless transmission paths and employing NOMA protocols to address spectrum shortage. This paper introduces a multi-objective optimization problem considering various parameters and utilizes deep reinforcement learning (DRL) algorithms to achieve real-time interaction with the communication environment. Transitioning to [25], the focus shifts to studying the performance of RIS-assisted networks in the presence of hardware impairments and interference, providing analytical expressions for outage probability (OP) and conducting asymptotic analysis to evaluate system performance under high signal-to-noise ratios (SNRs). Lastly, [23] explores the role of user clustering techniques in optimizing resource allocation and enhancing network performance in NOMA-based communication. It organizes and categorizes various clustering methods, highlighting their applicability in diverse communication scenarios. These papers collectively contribute to advancing our understanding and optimizing the deployment of RIS in next-generation wireless networks, addressing challenges such as covert communications, dynamic network environments, hardware impairments, and resource allocation optimization.

The improvement has not only restricted to the communication functionality but also has been extended to the sensing functionality and furthermore has been exported to ISAC systems [11, 12, 26]. One of the main advantages of the RIS is its ability to improve the performance of the wireless systems while being almost passive in terms of energy consumption [5, 13]. In [13], the authors have developed energy-efficient designs for both the transmit power allocation and the RIS passive beamforming for RIS-aided downlink multi-user MISO system, under maximum power and individual quality of service (QoS) constraints for the users. Their developed algorithms are proven to provide higher EE compared with relay-assisted communication system. In [5], the authors have investigated the resource allocation problem for wireless networks with spatially distributed RISs. Specifically, under minimum rate constraints of the users, they maximized the EE of a network with spatially distributed RISs that are used to serve multiple wireless users, through optimizing the on–off status of each RIS as well as the passive beamforming matrix of the RISs.

The comparison between active RISs and relays employing active transmitting antenna underscores several fundamental differences in their functionality and implementation. Firstly, in terms of hardware complexity, relays necessitate active electronic components like digital-to-analog converters (DACs) and power amplifiers, leading to higher costs and power consumption, especially for multiple-antenna designs. Conversely, active RISs, comprising metallic or dielectric patches on a grounded substrate, rely on low-power electronic circuits for configurability and Zener diode for implementing a reflection-type amplifier, resulting in lower complexity and potential cost savings, as demonstrated by recent large-scale prototypes. Regarding noise, while relays are susceptible to additive noise and self-interference, active RISs functioning

as anomalous reflectors is unaffected by additive noise but may encounter phase noise limitations and controlled dynamic noise that is affected by the amplification gain which in any cases is not comparable with the noise generated in relays with transmitting antennas. Spectral efficiency comparisons reveal that relay systems are constrained by half-duplex operation and self-interference, whereas active RISs offer more flexibility in signal combination and can optimize surface reflection coefficients. Power-wise, relays require dedicated power sources, while active RISs can operate with minimal dynamic power source for configurability of both the reflection and amplification gains, with power allocation being integral to both systems but in differing manners. Additionally, the scaling of average signal-to-noise ratio with the number of elements differs between relays and RISs, with RISs exhibiting quadratic scaling in far-field scenarios due to their unique reflective properties. However, the comparison's implications on performance are nuanced, considering factors such as path loss and transmission distance. Overall, this comprehensive comparison highlights the distinct advantages and considerations associated with both active RISs and relays in wireless communication systems.

Active RISs [10, 27] permit to overcome the double path-loss effect at the price of increased energy consumption for amplification of the reflected signal. The power consumption model in active-RIS is different from that of passive RIS, which motivates us study the EE in ISAC scenarios with active-RISs [28]. The state-of-the-art works related to active and passive RIS-based communication and sensing are discussed in [29]. Although the RIS has indicated great potentials with both the communication and sensing applications, it has been realized that passive version of the RIS suffers from the so-called *double fading or multiplicative fading* effect[1] [30]. One method to alleviate the multiplicative fading effect is to deploy the RIS very close to either the transmitter or the receiver, but this severely restricts the coverage range of the passive RIS [27]. Active RIS has recently been introduced to combat the multiplicative fading effect, and the improvements accompanying its deployment are investigated for both the communication and sensing applications [10, 27, 31, 32]. With active-RIS, each RIS element is equipped with reflection-type amplifier to enlarge the reflected signal which in turn overcomes the multiplicative fading effect while still maintain its low complexity at the cost of slight increase in the power consumption. Since the power consumption model in active-RIS is different than its passive RIS counterpart, the study of the EE of wireless networks that involve both communication and sensing functionalities with active-RIS will be highly challenging and worth investigation.

This paper addresses the challenge of maximizing communication EE within an ISAC downlink system employing an active RIS. Our work leverages a dual-function base station capable of performing MU-MISO communication while concurrently sensing a target with the aid of the active RIS. We formulate an optimization problem to maximize the system's EE by jointly optimizing power allocation and the active beamforming of the RIS. This optimization considers individual user rate

---

[1] This means that the reflected signal, which suffers an accumulated attenuation through the cascaded channel from the transmitter to the receiver through the RIS, is generally several orders of magnitude smaller than that following the direct path from the transmitter to the receiver.

requirements, minimum beampattern gains toward the sensing direction, and power constraints related to the active RIS. The key novelty lies in our approach to solving this complex fractional programming problem. We propose an alternating optimization algorithm that effectively decouples the optimization variables. This allows us to decompose the problem into two manageable sub-problems: active beamforming and power allocation. For the beamforming problem, we introduce two novel algorithms based on Nested Fractional Programming (NFP) and Sequential Fractional Programming (SFP). Additionally, we present a solution to the power allocation problem using Dinkelbach's algorithm. Extensive simulations validate the effectiveness of our proposed alternating optimization framework. Our work demonstrates that the power allocation and RIS beamforming algorithms can achieve an 85% increase in communication EE compared to a baseline system, all while allocating sufficient propping power for target sensing over line-of-sight (LoS) channels, within the same total power budget.

The remaining part of this paper is organized as follows. Section contains the system and signal models, along with the formulation of the considered optimization problem. Section presents the proposed algorithms, while simulation results are investigated in Sect. . Finally, concluding remarks are given in Sect. .

Notation: Matrices and vectors are denoted by boldface upper case and lower case, respectively. $(\cdot)^H$ and $(\cdot)^{-1}$ are the matrix Hermitian and the inverse, respectively. $|\cdot|$, $\|\cdot\|_F$, and $\text{tr}(\cdot)$ denote modulus, Frobenius norm, and matrix trace. $j = \sqrt{-1}$ is the imaginary unit and $\mathbb{C}$ is the set of complex numbers. $\mathcal{CN}(0, \sigma^2)$ is a zero-mean complex circularly symmetric Gaussian random variable with variance σ^2.

The list of abbreviations in the paper is listed in Table 1 at the end of the paper.

Table 1 List of abbreviations

The technical term	The abbreviation
Additive White Gaussian Noise	AWGN
Alternating Optimization	AO
Convex Optimization Toolbox	CVX
Direct Current	DC
Dual-Functional Radar and Communication Base-Station	DFRC-BS
Energy Efficiency	EE
Integrated Sensing and Communications	ISAC
Multiple Input Multiple Output	MIMO
Multiple Input Single Output	MISO
Sixth Generation Mobile Communication System	6G
Multi-user Multiple Input Single Output	MU-MISO
Nested Fractional Programming	NFP
Quality of Service	QoS
Reconfigurable Intelligent Surface	RIS
Spectral Efficiency	SE
Sequential Fractional Programming	SFP
Signal to Interference plus Noise Ratio	SINR
Uniform Linear Array	ULA
Zero-Forcing	ZF

Rihan *et al. J Wireless Com Network*   (2024) 2024:20

Page 6 of 22

2 System model

As shown in Fig. 1, we consider a RIS-assisted ISAC system that consists of a dual-functional radar and communication basestation (DFRC-BS) equipped with an uniform linear array (ULA) of M antennas that serves K-single antenna users on the downlink while simultaneously sensing a target in a given range-cell. An active RIS with N elements is deployed close to the mobile users to improve the overall system performance. It is assumed that the target is located far-away from the RIS so that the RIS does not impact the sensing task but only helps in improving the communication system performance. The direct communication channel between the DFRC-BS and the users is available, but they are degraded due to unfavorable propagation conditions.

We denote by $\mathbf{h}_{d,k} \in \mathbb{C}^{1 \times M}$ and $\mathbf{h}_{r,k} \in \mathbb{C}^{1 \times N}$ the direct communication channels between the DFRC-BS and the user k and between the RIS and the user k, respectively. Moreover, the matrix $\mathbf{G} \in \mathbb{C}^{N \times M}$ represents the channel between the DFRC-BS and the RIS, while the diagonal matrix $\Phi = \text{diag}[\phi_1, \phi_2, \ldots, \phi_N]$ represents the active RIS configuration. Despite the inherent challenges in assuming the availability of perfect CSI in passive RIS scenarios, the utilization of active RIS justifies the assumption of possessing perfect CSI knowledge within our scenario [33]. This justification is reinforced by the existence of contemporary channel estimation approaches that can significantly leverage the deployment of active RIS [34]. Notice that $\phi_n = a_n e^{j\theta_n}$, with a_n a positive real amplification factor for the n-th element of the RIS. We assume that $\Phi = \mathbf{A}\Theta$, with $\mathbf{A}$ and Θ diagonal matrices, containing on their diagonal the coefficients a_n and $e^{j\theta_n}$, respectively,
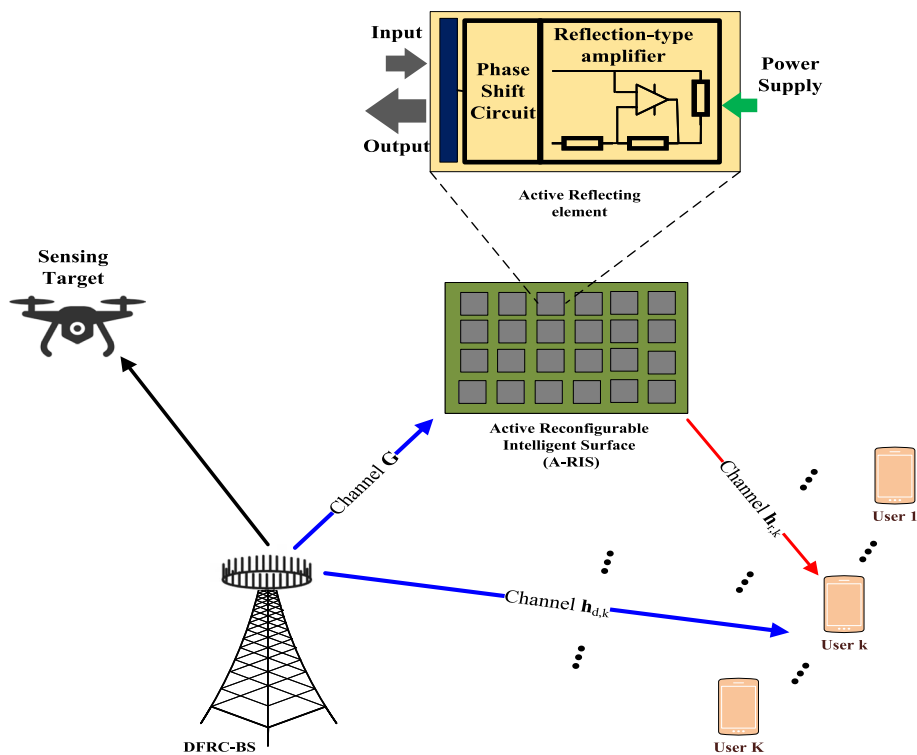

Fig. 1 Active RIS-assisted multiuser ISAC system

$\forall n$. While we acknowledge that assuming infinite phase shift resolution may not fully reflect real-world scenarios, it was adopted for simplification purposes to establish theoretical foundations and facilitate analytical tractability, with a focus on studying EE. To provide further justification for this assumption, we summarize the outcomes of [35]. It has been mathematically demonstrated that, even with a modest number of RIS elements (e.g., 3), the performance degradation resulting from assuming continuous phase shift is less than 10% with only 3 bits. Furthermore, when increasing the number of RIS elements to 300 while maintaining the same 3-bit resolution, the performance degradation drops to below 1%. Consequently, for scenarios involving a moderate number of reflecting elements, assuming continuous phase shift results in a performance degradation of up to 1%, while significantly enhancing analytical tractability.

Then, $\mathbf{h}_k = \left(\mathbf{h}_{d,k} + \mathbf{h}_{r,k} \Phi \mathbf{G} \right) \in \mathbb{C}^{1 \times M}$ denotes the composite channel from the DFRC-BS to user k. Letting $s_1, \ldots, s_K$ be the unit-energy K information symbols, and s_0 an unit-energy fictitious data symbol to be associated with the sensing beam, the discrete-time version of the signal transmitted by the DFRC-BS is $\mathbf{x} \triangleq \sum_{k=1}^{K} \sqrt{p_k} \mathbf{w}_k s_k + \sqrt{p_0} \mathbf{w}_0 s_0$ where p_k and $\mathbf{w}_k$ are the transmit power, and the precoding vector associated with the k-th beam. The vector $\mathbf{x}$ is subject to a power budget constraint, such that $E[|\mathbf{x}|^2] = \mathrm{tr}(\mathbf{P}\mathbf{W}^H\mathbf{W}) \leq P_{\max}$, where $\mathbf{W} \triangleq [\mathbf{w}_0, \mathbf{w}_1, \mathbf{w}_2, \ldots, \mathbf{w}_K] \in \mathbb{C}^{M \times (K+1)}$, $\mathbf{P} \triangleq \mathrm{diag}[p_0, p_1, p_2, \ldots, p_K] \in \mathbb{R}^{(K+1) \times (K+1)}$.

The discrete-time signal received at the k-th mobile user can be expressed as $y_k = \mathbf{h}_k \mathbf{x} + \mathbf{h}_{r,k} \Phi \mathbf{G} \mathbf{n}_{\mathrm{RIS}} + n_k$, where $n_k \sim \mathcal{CN}(0, \sigma^2)$ is the additive white Gaussian noise (AWGN) at user k, and the vector $\mathbf{n}_{\mathrm{RIS}} \sim \mathcal{CN}\left(\mathbf{0}_N, \sigma_{\mathrm{RIS}}^2 \mathbf{I}_N \right)$ denotes the dynamic noise introduced by the active-RIS. The signal to interference plus noise ratio (SINR) at user k is[2]

$$\gamma_k = \frac{p_k |\mathbf{h}_k \mathbf{w}_k|^2}{p_0 |\mathbf{h}_k \mathbf{w}_0|^2 + \sum\limits_{i=1, i \neq k}^{K} p_i |\mathbf{h}_k \mathbf{w}_i|^2 + \sigma_{\mathrm{RIS}}^2 \left\| \mathbf{h}_{r,k} \Phi \right\|_2^2 + \sigma^2}. \tag{1}$$

Then, the communication spectrum efficiency in (bps/Hz) is given based on (1) by $\mathcal{R} \triangleq \sum_{k=1}^{K} \log(1 + \gamma_k)$. We are assuming that the DFRC-BS is simultaneously working in the tracking mode to sense a target at an azimuth angle of ϕ in addition to provide the communication service to K users. The probing power used to track the target at angle ϕ is $P_r = M^{-1} \mathbf{a}^H(\phi) \mathbf{W} \bar{\mathbf{P}} \mathbf{W}^H \mathbf{a}(\phi) = \mathbf{a}^H(\phi) \mathbf{W} \mathbf{P} \mathbf{W}^H \mathbf{a}(\phi)$, where the vector $\mathbf{a}(\phi) \in \mathbb{C}^{M \times 1}$ denotes the transmit steering vector in the direction of angle ϕ, and $\mathbf{P} = M^{-1} \bar{\mathbf{P}}$. Since the DFRC-BS employs an ULA, the steering vector $\mathbf{a}(\phi)$ can be written as $\mathbf{a}(\phi) = \left[1, e^{j\frac{2\pi d}{\lambda} \sin(\phi)}, \ldots, e^{j\frac{2\pi d}{\lambda}(M-1)\sin(\phi)} \right]^T$, where d is the array inter-element spacing and λ represent the signal wavelength. Without loss of generality, it is assumed that $d = \frac{\lambda}{2}$.

---

[2] If $\sigma_{\mathrm{RIS}}^2 = 0$, $a_n = 1$ for all n, the model reduces to a passive RIS.

2.1 Total power consumption model

The total power consumption model to be considered in this work consists of the DFRC-BS transmit power, plus the hardware static power dissipated in the DFRC-BS, user terminals, and the active RIS. We have thus $\mathcal{P}_{\text{total}} = \sum_{k=1}^{K} \left(\xi p_k + P_{UE,k} \right) + P_{BS} + P_{\text{RIS,a}}$. In this relation, ξ is the efficiency of the transmit power amplifier; $P_{UE,k}$ is the power dissipated in the hardware of the k-th communication user terminal. Additionally, P_{BS} and $P_{\text{RIS,a}}$ denote the total static power dissipated at the DFRC-BS and in the active RIS, respectively. Regarding P_{BS}, we assume that the DFRC-BS transmit power amplifier operates in the linear region so that its circuit power does not depend on the communication rate [4]. The power consumption in the active RIS depends on the number of reflective elements and the phase shift resolution of its reflecting elements [27], so it can be expressed as $P_{\text{RIS,a}} = N(P_c(b) + P_{DC}) + \xi_{\text{RIS,a}} P_{\text{out}}$, where $P_c(b)$ is the static power consumption for each reflective element with b bits resolution,[3] while the power P_{DC} represents the DC biasing power consumption for each reflective element. The coefficient $\xi_{\text{RIS,a}}$ represents the active RIS amplifier efficiency, while the output power from the active RIS can be expressed as, $P_{\text{out}} = \|\Phi \mathbf{G} \mathbf{P}\|_F^2 + \sigma_{\text{RIS,a}}^2 \|\Phi \mathbf{I}_N\|_F^2$.

2.2 Methods and problem formulation

Our main objective is to optimize, with respect to the matrices $\mathbf{P}$ and Φ, the system's communication EE, defined as follows:

$$\eta_{\text{EE}} = \frac{B \sum_{k=1}^{K} \log_2 \left(1 + \gamma_k \right)}{\mathcal{P}_{\text{total}}} , \tag{2}$$

with B referring to the signal bandwidth. To avoid trivial solutions, the maximization of the EE is to be carried out under power budget constraints and QoS constraints for the communication and sensing tasks. In the following, in order to come up with a tractable problem, we assume that the phase shifters of the RIS can have infinite resolution and that all the channels in the scenario are perfectly known at the DFRC-BS. Moreover, we assume that the communication beamformers $\mathbf{w}_1, \ldots, \mathbf{w}_K$ are designed according to a Zero-Forcing (ZF) criterion, so that the interfering terms in the denominator of the SINR in (1) disappear and only the AWGN-related last two summands survive. As to the sensing beamformer $\mathbf{w}_0$, denoting by δ the angle, with respect to the DFRC-BS antenna array, of the range cell under test, we assume that $\mathbf{w}_0$ is the normalized response of the DFRC-BS antenna array at the angle δ. Denoting by $\mathbf{W}_{ZF}$ an $[M \times (K+1)]$-dimensional matrix containing the $K+1$ beamformers on its columns, the EE maximization problem can be expressed as follows

$$\max_{\mathbf{P},\Phi} \eta_{\text{EE}}(\mathbf{W}_{ZF})$$

$$\text{s.t.} B \log_2 \left(1 + \frac{p_k}{\sigma_{\text{RIS}}^2 \|\mathbf{h}_{r,k} \Phi\|^2 + \sigma^2} \right) \geq R_{\min,k} , \forall k \tag{3a}$$

---

[3] Discrete phase shifts achieve similar performance as continuous ones if a resolution of at least 6 bits is used. Thus, we assume continuous phase shifts with a power value of 7.8 mW per element, which is equivalent to 6-bit resolution [4]

$$\mathbf{a}^H(\delta)\mathbf{W}_{ZF}\mathbf{P}\mathbf{W}_{ZF}^H\mathbf{a}(\delta) \leq \eta P_{\max}, \tag{3b}$$

$$\mathrm{tr}(\mathbf{W}_{ZF}\mathbf{P}\mathbf{W}_{ZF}^H) \leq P_{\max}, \tag{3c}$$

$$\|\boldsymbol{\Phi}\mathbf{G}\mathbf{P}\|_F^2 + \sigma_{\mathrm{RIS,a}}^2\|\boldsymbol{\Phi}\mathbf{I}_N\|_F^2 \leq P_a. \tag{3d}$$

where P_a is the power budget at the active RIS, $R_{\min,k}$ denotes the QoS constraint for each individual communication user k as shown in constraint (3a), and $\eta_{\mathrm{EE}}(\mathbf{W}_{\mathrm{ZF}})$ is the EE function in (2) while employing the ZF beamformer. Also, constraint (3b) is used to guarantee that the sensing power toward the direction δ is upper-bounded by $P_s = \eta P_{\max}$, with $0 \leq \eta \leq 1$ is the portion of the DFRC power allocated for radar sensing functionality. This parameter leverages the trade-off between the communication and sensing functionalities that share the same power budget, allocating η of this budget for sensing and $(1 - \eta)$ of the budget for communication. Constraint (3c) ensures that the DFRC-BS transmit power remains below the maximum feasible threshold $P_{\max}$. In constraint (3d), the power budget at the active RIS is satisfied.

3 Communication EE optimization

Problem (3) is challenging due to (3b)–(3c). A tractable approach is to decouple the optimization variables and employ alternating optimization (AO) [36], with respect to $\boldsymbol{\Phi}$ with constant $\mathbf{P}$, and to $\mathbf{P}$ with constant $\boldsymbol{\Phi}$. Since η_{EE} is upper-bounded over the feasible set, the AO must eventually converge in the value of the objective.

3.1 Optimization with respect to $\boldsymbol{\Phi}$

Before going into the mathematical details of the case of fixed $\mathbf{P}$, let us talk about of Dinkelbach's algorithm. Dinkelbach's algorithm is a powerful iterative optimization technique used conventionally to solve fractional programming problems. The algorithm is particularly effective in situations where the objective function involves a ratio of two convex functions. Dinkelbach's algorithm iteratively solves a series of modified optimization problems, each of which involves replacing the original fractional objective function with a simpler, equivalent function. At each iteration, the algorithm converges toward the optimal solution by solving the modified problem and updating the solution accordingly. One of the key advantages of Dinkelbach's algorithm is its ability to handle fractional programming problems efficiently and converge to the globally optimal solution under certain conditions.

For fixed $\mathbf{P}$, the problem in (3) reduces to:

$$\max_{\boldsymbol{\Phi}} \frac{\sum_{k=1}^K \log_2\left(1 + \frac{p_k}{\sigma^2}\left(1 + \frac{\sigma_{\mathrm{RIS}}^2}{\sigma^2}\left\|\mathbf{h}_{r,k}\boldsymbol{\Phi}\right\|_2^2\right)^{-1}\right)}{\xi_{\mathrm{RIS,a}}\left(\|\boldsymbol{\Phi}\mathbf{G}\mathbf{P}\|_F^2 + \sigma_{\mathrm{RIS,a}}^2\|\boldsymbol{\Phi}\mathbf{I}_N\|_F^2\right) + C_1} \tag{4a}$$

$$\mathrm{s.t.}\left\|\mathbf{h}_{r,k}\boldsymbol{\Phi}\right\|_2^2 \geq \sigma_{\mathrm{RIS}}^{-2}\left(p_k(2^{R_{\min,k}} - 1)^{-1} - \sigma^2\right), \forall k$$

$$\|\Phi\mathbf{GP}\|_F^2 + \sigma_{\text{RIS,a}}^2\|\Phi\mathbf{I}_N\|_F^2 \leq P_a. \tag{4b}$$

with $C_1 = \sum_{k=1}^K \left(\xi p_k + P_{UE,k}\right) + P_{BS} + N(P_c(b) + P_{DC})$. Let $R_k(\Phi)$ denote each summand in the numerator of (4).

Since $R_k(\Phi)$ is not concave, Dinkelbach's algorithm cannot be used directly. Then, we propose two approaches.

3.1.1 Nested Fractional Programming

This approach consists of a reformulation procedure involving an external fractional program for the EE ratio and an internal fractional program for the SINR terms at the EE numerator. We apply the quadratic transform from [37 1] to decouple the EE as:

$$F_q = 2y\left(\sum_{k=1}^K R_k(\Phi)\right)^{\frac{1}{2}} - y^2\left(\xi_{\text{RIS,a}}\left(\|\Phi\mathbf{GP}\|_F^2 + \sigma_{\text{RIS,a}}^2\|\Phi\|_F^2\right) + C_1\right). \tag{5}$$

This reformulated objective is not concave over Φ, due to the first summand. Then, we apply the quadratic transformation also to each SINR term in $F_q(\Phi)$, and further recast F_q as F_{qq} as:

$$
\begin{aligned}
F_{qq}(\Phi, y) = {}& 2y\left(\sum_{k=1}^K \log\left(1 + 2p_k\text{Re}\{z_k\} - z_k^H\left(\sigma^2 + \sigma_{\text{RIS}}^2\|\mathbf{h}_{r,k}\Phi\|_2^2\right)z_k\right)\right)^{\frac{1}{2}} \\
& - y^2\left(\xi_{\text{RIS,a}}\left(\|\Phi\mathbf{GP}\|_F^2 + \sigma_{\text{RIS,a}}^2\|\Phi\mathbf{I}_N\|_F^2\right) + C_1\right).
\end{aligned}
\tag{6}
$$

The optimization problem in (4) can ultimately be reformulated after the two uses of the quadratic transform into:

$$\underset{\Phi, y, \mathbf{z}}{\text{maximize}}\ F_{qq}\left(\Phi, y, \mathbf{z}\right)$$
$$\text{s.t.}\ \left\|\mathbf{h}_{r,k}\Phi\right\|_2^2 \geq \sigma_{\text{RIS}}^{-2}\left(p_k(2^{R_{\min,k}} - 1)^{-1} - \sigma^2\right), \forall k \tag{7a}$$

$$\|\Phi\mathbf{GP}\|_F^2 + \sigma_{\text{RIS,a}}^2\|\Phi\mathbf{I}_N\|_F^2 \leq P_a\ ,\mathbf{z} \in \mathbb{C}^N \tag{7b}$$

where $\mathbf{z} = \{z_k\}_k$. We note that y and $\mathbf{z}$ are the auxiliary variables introduced in the first and second fractional programming, respectively. For fixed Φ and y, the optimal z_m is:

$$z_k^\star = p_k\left(\sigma^2 + \sigma_{\text{RIS}}^2\|\mathbf{h}_{r,k}\Phi\|_2^2\right)^{-1}, \forall k. \tag{8}$$

After updating the variable $\mathbf{z}$, the optimal y is given as:

$$y^\star = \frac{\sqrt{\sum_{k=1}^K R_k(\Phi)}}{\xi_{\text{RIS,a}}\left(\|\Phi\mathbf{GP}\|_F^2 + \sigma_{\text{RIS,a}}^2\|\Phi\mathbf{I}_N\|_F^2\right) + C_1}. \tag{9}$$

Finally, when $\mathbf{z}$ and y are both fixed, the optimization problem in (7) is a convex problem of Φ and can easily be solved using standard numerical tools such as CVX. The convergence of Algorithm 1 that solves the problem in (7) is guaranteed according to [37].

Algorithm 1 Nested Fractional Programming for Optimizing Φ

1: **Initialization:** Initialize $\boldsymbol{\Phi}$ to a feasible value.
2: Repeat
3:          Update $\mathbf{z}$ by (8) and y by (9).
4:          Update $\boldsymbol{\Phi}$ by solving (7) for fixed y and $\mathbf{z}$.
5: **until** the value of the function F_{qq} in (6) converges.

3.1.2 Sequential Fractional Programming

To apply the sequential method, a concave lower bound of the numerator of the EE is needed. This can be achieved by the inequality, $\log(1 + \frac{x}{y}) \geq \log(1 + \frac{\bar{x}}{\bar{y}}) + \frac{\bar{x}}{\bar{y}}(\frac{2\sqrt{x}}{\sqrt{\bar{x}}} - \frac{x+y}{\bar{x}+\bar{y}} - 1)$, which holds for any x, y, $\bar{x}$, and $\bar{y}$, and holds with equality if and only if $x = \bar{x}$ and $y = \bar{y}$. Let us use $x = \bar{x} = p_k$, and $y = \sigma^2 + \sigma_{\text{RIS}}^2 \lVert \mathbf{h}_{r,k}\Phi \rVert_2^2$, and $\bar{y} = \sigma^2 + \sigma_{\text{RIS}}^2 \lVert \mathbf{h}_{r,k}\bar{\Phi} \rVert_2^2$ with $y \neq \bar{y}$ or $\Phi \neq \bar{\Phi}$, where Φ is any feasible RIS reflection matrix. We obtain

$$
\begin{aligned}
\log_2 &\left(1 + \frac{p_k}{\sigma^2 + \sigma_{\text{RIS}}^2 \lVert \mathbf{h}_{r,k}\Phi \rVert_2^2}\right) \geq \log_2\left(1 + \frac{p_k}{\sigma^2 + \sigma_{\text{RIS}}^2 \lVert \mathbf{h}_{r,k}\bar{\Phi} \rVert_2^2}\right) \\
&+ \frac{p_k}{\left(\sigma^2 + \sigma_{\text{RIS}}^2 \lVert \mathbf{h}_{r,k}\bar{\Phi} \rVert_2^2\right)}\left(1 + \frac{p_k + \sigma^2 + \sigma_{\text{RIS}}^2 \lVert \mathbf{h}_{r,k}\Phi \rVert_2^2}{p_k + \sigma^2 + \sigma_{\text{RIS}}^2 \lVert \mathbf{h}_{r,k}\bar{\Phi} \rVert_2^2}\right)
\end{aligned}
\tag{10}
$$

By utilizing the lower bound of the concave function on the right-hand side of (10) and employing a simple linearization technique to the term $\lVert \mathbf{h}_{r,k}\Phi \rVert_2^2$ in constraint (4a), the optimization problem presented in (4) can be transformed into a concave maximization problem subject to convex constraints. This transformed problem can be efficiently solved using the Sequential Fractional Programming approach [38].

3.2 Optimization with respect to the power allocation matrix

For fixed Φ, the problem in (3) reduces to:

$$
\max_{\mathbf{P}} \frac{\sum_{k=1}^{K} \log_2\left(1 + p_k\left(\sigma_{\text{RIS}}^2 \lVert \mathbf{h}_{r,k}\Phi \rVert_2^2 + \sigma^2\right)^{-1}\right)}{\xi \sum_{k=1}^{K} p_k + \xi_{\text{RIS,a}} \lVert \Phi \mathbf{GP} \rVert_F^2 + C_2}
\tag{11a}
$$
$$
\text{s.t.} p_k \geq (\sigma_{\text{RIS}}^2 \lVert \mathbf{h}_{r,k}\Phi \rVert_2^2 + \sigma^2)(2^{R_{min,k}} - 1), \forall k
$$

$$
\text{tr}(\mathbf{a}^H(\delta)\mathbf{W}_{\text{ZF}}\mathbf{PW}_{\text{ZF}}^H \mathbf{a}(\delta)) \leq \eta P_{\max},
\tag{11b}
$$

$$\text{tr}(\mathbf{W}_{\text{ZF}}\mathbf{P}\mathbf{W}_{\text{ZF}}^H) \leq P_{\max}, \tag{11c}$$

$$\|\boldsymbol{\Phi}\mathbf{G}\mathbf{P}\|_F \leq \sqrt{P_a - \sigma_{\text{RIS,a}}^2 \|\boldsymbol{\Phi}\mathbf{I}_N\|_F^2}. \tag{11d}$$

where $C_2 \sum_{k=1}^{K} P_{UE,k} + P_{BS} + N(P_c(b) + P_{DC}) + \xi_{\text{RIS,a}}\sigma_{\text{RIS,a}}^2 \|\boldsymbol{\Phi}\|_F^2$. The optimization problem in (11) is non-convex in general. However, for fixed $\boldsymbol{\Phi}$, the numerator of the objective function is concave in $\mathbf{P}$, while its denominator is convex in $\mathbf{P}$. Moreover, (11a), (11b), and (11c) are all affine constraints with respect to $\mathbf{P}$, while (11d) is a strictly convex constraint with respect to $\mathbf{P}$. Accordingly, problem (11) is a single-ratio concave-convex fractional problem and thus it can be globally solved by Dinkelbach's algorithm [37]. This method is summarized in Algorithm 2, where $\mathcal{B} \triangleq \{\mathbf{P} = \text{diag}[p_0, p_1, p_2, \ldots, p_K] : (11a) \cap (11b) \cap (11c) \cap (11d)\}$ and $\mathbf{P}_i^\star \triangleq \text{diag}[p_{0,i}^\star, p_{1,i}^\star, p_{1,i}^\star, \ldots, p_{K,i}^\star]$ refer to the transmit power allocation solution in Step 3 at each iteration.

Algorithm 2 Dinkelbach's algorithm to solve (11)

1: **Initialization:** $K, b, P_{DC}, P_{UE}, P_c(b), P_{BS}, \sigma^2, \sigma_{\text{RIS}}^2, \xi, \xi_{\text{RIS,a}}, P_a, \mathbf{G}, \epsilon > 0, \lambda_0 = 0, \mathbf{h}_{r,k}, \boldsymbol{\Phi}_k \forall k = 1, 2, \cdots, K.$
2: **for** $i = 1, 2, \cdots$ **do**
3:     Solve the concave maximization:

$$\mathbf{P}_i^\star = \underset{\mathbf{P} \in \mathcal{B}}{\arg\max} \sum_{k=1}^{K} \log_2 \left(1 + p_k \left(\sigma_{\text{RIS}}^2 \|\mathbf{h}_{r,k}\boldsymbol{\Phi}\|_2^2 + \sigma^2\right)^{-1}\right)$$
$$- \lambda_{i-1} \left(\xi \sum_{k=1}^{K} p_k + \xi_{\text{RIS,a}} \|\boldsymbol{\Phi}\mathbf{G}\mathbf{P}\|_F^2 + C_2\right).$$

4:     Set:

$$\lambda_i = \frac{\sum_{k=1}^{K} \log_2 \left(1 + p_{k,i}^\star \left(\sigma_{\text{RIS}}^2 \|\mathbf{h}_{r,k}\boldsymbol{\Phi}\|_2^2 + \sigma^2\right)^{-1}\right)}{\xi \sum_{k=1}^{K} p_{k,i}^\star + \xi_{\text{RIS,a}} \|\boldsymbol{\Phi}\mathbf{G}\mathbf{P}^\star\|_F^2 + C_2}$$

5:     **if** $|\lambda_i - \lambda_{i-1}| < \epsilon$ **then**
6:         **Output:** $\mathbf{P}_i^\star$.
7:     **end if**
8: **end for**

Let us denote the number of iterative gradient updates in the Nested and Sequential FP algorithms for the RIS phase-shift optimization sub-problem as I_{nest} and I_{seq}, respectively, and the number of iterations of Dinkelbach's algorithm for transmit power optimization as I_{din}. Consequently, the Nested FP and Sequential FP algorithms for the active-RIS scenario exhibit maximum asymptotic complexities of $\mathcal{O}\big(I_{\text{am}}(2I_{\text{nest}}MN^5 + I_{\text{din}}K^4)\big)$, and $\mathcal{O}\big(I_{\text{am}}(I_{\text{seq}}MN^4 + I_{\text{din}}K^4)\big)$, respectively. On the

other hand, the complexities of the proposed nested FP and sequential FP with a passive RIS are $\mathcal{O}\big(I_{\mathrm{am}}\big(I_{\mathrm{nest}}N^3 + I_{\mathrm{din}}K^4\big)\big)$, and $\mathcal{O}\big(I_{\mathrm{am}}\big(I_{\mathrm{seq}}N^2 + I_{\mathrm{din}}K^4\big)\big)$, respectively.

4 Results and discussion

We used MATLAB to simulate the considered system with $K = 8$ users and a radar target at angle $60°$, with the positions of all components shown in Fig. 2. The single-antenna users are randomly distributed inside a circle of radius 25 m centered at $(200m, 0)$. All the results are averaged over 10^4 users' positions and channel realizations. The channels between the DFRC-BS and RIS follow the Rician fading channel model [39], with Rician factor α. Additionally, we assume the channels between the DFRC-BS and users, and between the RIS and users, follow the Rayleigh model with path-loss exponents 3.5 and 2, respectively [40]. Simulation parameters are in Table 2, unless specified otherwise [4, 27]. We assume $R_{\mathrm{min},k} = R_{\mathrm{min}}$ for all k and we set R_{min} to be a fraction of the rate that each user would attain in the ideal case of mutually orthogonal channels and uniform power allocation. We compare the Nested Fractional Programming (Nested FP), Sequential Fractional Programming (sequential FP), and the case of passive RIS presented in [4] with the same power budget. The table also includes the circuit dissipation power parameters for BS, RIS, and the mobile users based on [4, 27].
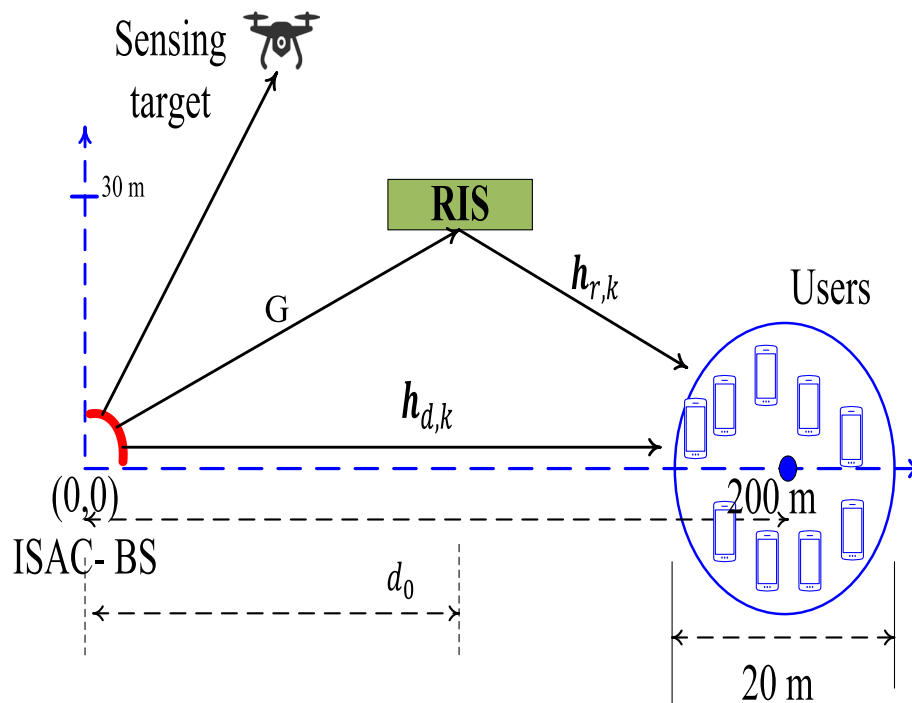
Fig. 2 The considered simulation setup

Table 2 Simulation parameters

Parameters	Values
RIS central element placement	$(d_0, 30\text{m})$
DFRC-BS element placement	(0,0)
Small-scale fading model for all channels	$\in \mathcal{CN}(0,1)$
Large-scale fading model at distance d	$\frac{10^{-3.53}}{d^{3.76}}$
Transmission bandwidth B	15 MHz
Algorithmic convergence parameter ϵ	10^{-4}
DC power consumption for each active RE P_{DC}	-8 dBm
Active RIS dynamic noise power	-134 dBm
Circuit dissipated power at DFRC-BS P_{BS}	1.5 dBW
Circuit dissipated power coefficients at DFRC-BS ξ	1.25
Maximum transmit power at DFRC-BS P_{max}	4.0 dBW
Dissipated power at each user $P_{UE,k}$	10 dBm
Dissipated power for active and passive RIS element	10 and 8 dBm
Power of background noises at users and RIS $\sigma^2 = \sigma_{RIS}^2$	-80 dBm
The maximum active RIS power budget	$10\% P_{max}$
Circuit dissipated power coefficients at the RIS $\xi_{RIS,a}$	1.25

Figure 3 shows the communication EE of active and passive RIS-based systems as a function of the maximum transmit power budget P_{max}, where the minimum rate constraint is set to zero. The proposed active RIS system outperforms its passive counterpart, and both systems achieve higher communication EE when a lower proportion of power, η, is allocated for sensing. This shows the trade-off between the communication and sensing functionalities that compete for a shared power budget. The active and passive RIS-based systems reach a saturation point in terms of their communication EE performance when the maximum transmit power of the ISAC is greater than or equal to 26 dBm. Beyond this limit, any power used in communication, sensing, and hardware circuitry in the DFRC-BS, RIS, and mobile users is not utilized, to avoid decreasing the communication EE of the system. Since the EE and spectrum efficiency (SE) are related through $(EE = (B \times SE)/P_{max})$, such a behavior of SE versus P_{max} was expected, as confirmed in Fig. 5.

Figure 4 shows how different R_{min} values affect the communication EE. Although both systems follow a similar trend, the active RIS system performs better in terms of communication EE. In some channel scenarios, the design problems were deemed infeasible, and the rate constraint was removed to analyze the system's behavior under extreme conditions. At low P_{max} values, both systems achieve low communication EE due to the insufficient transmit power. As P_{max} increases beyond 16 dBm while enforcing strict QoS constraints, the communication EE decreases faster due to the excess ISAC base station power allocated to meet the user rate constraint.
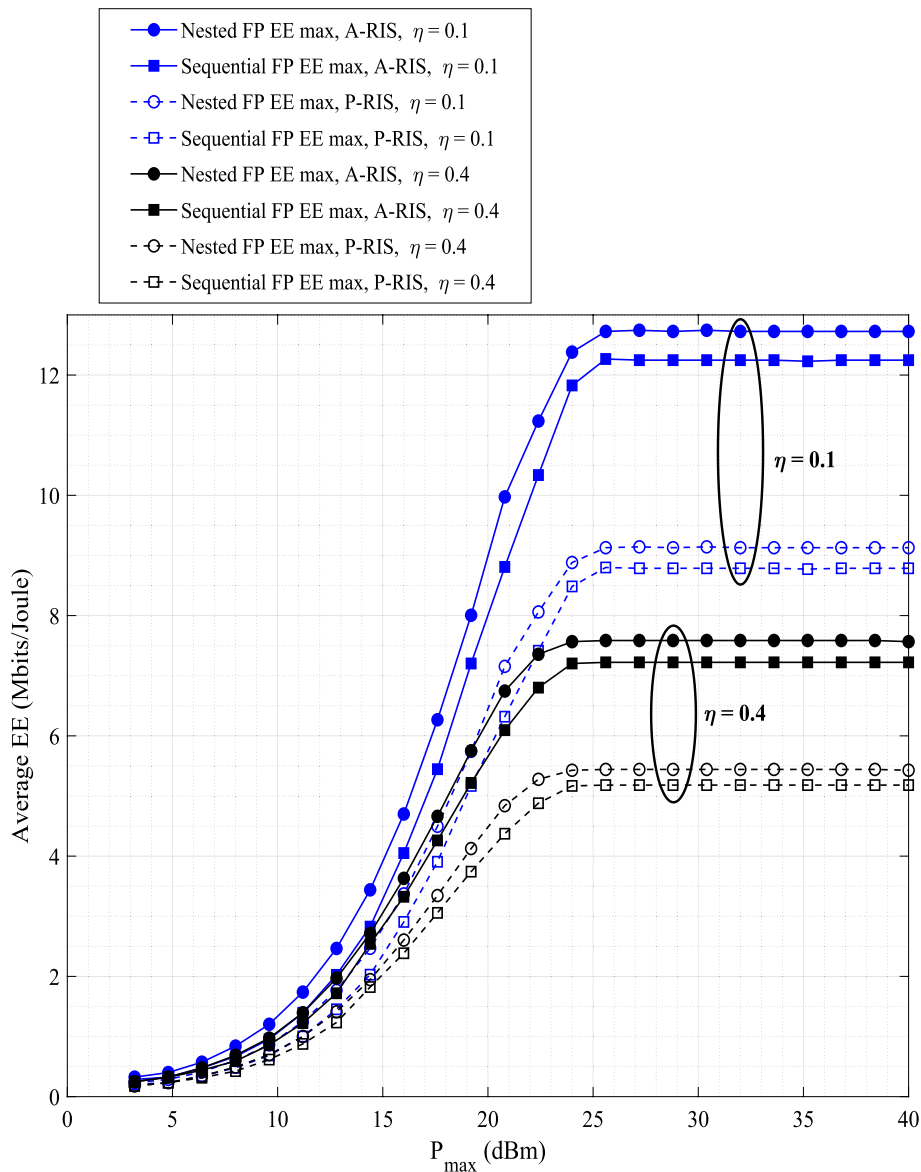
Fig. 3 Average communication EE versus P_{max} for $R_{min} = 0$ bits/Hz with $N = 64$, $P_c(b) = 7.8$mW, $M = 64$, $K = 8$

Figure 6 illustrates how the communication EE of active and passive RIS systems changes with circuit dissipated power consumption of each reflecting element $P_c(b)$, while considering different number of reflecting elements N. Figure 6 demonstrates the existence of an intersection point between the EE curves of active and passive RIS designs with each value of N. Therefore, there is a trade-off between
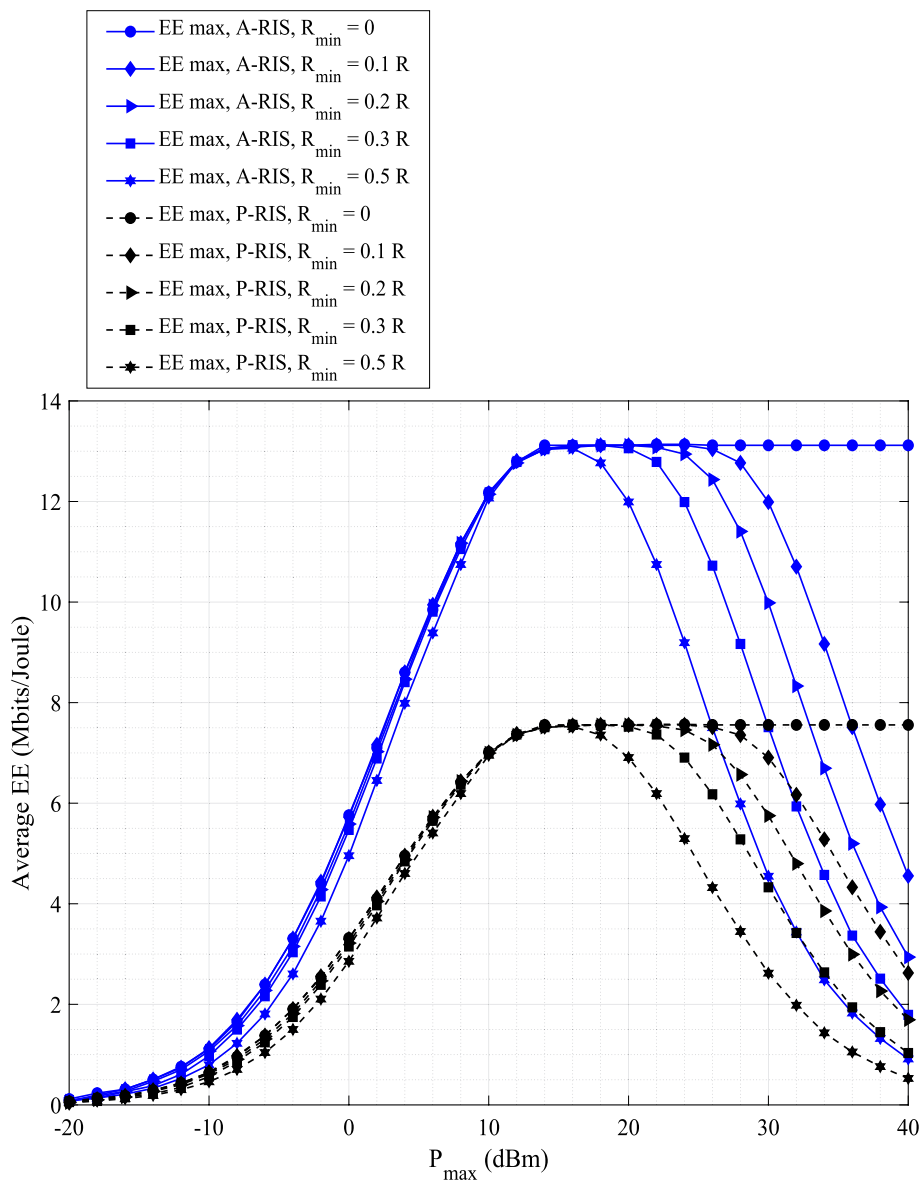
Fig. 4 Average communication EE versus $P_c(b)$ for different number of reflecting elements $N, M = 64, K = 8$

the rate improvement achieved by deploying a large number of reflecting elements and the effect on the system's communication EE. Similar conclusions can be drawn from Fig. 8 that shows the effect of increasing the number of RIS elements and accordingly the power consumption related to $P_c(b)$ on the communication EE performance.
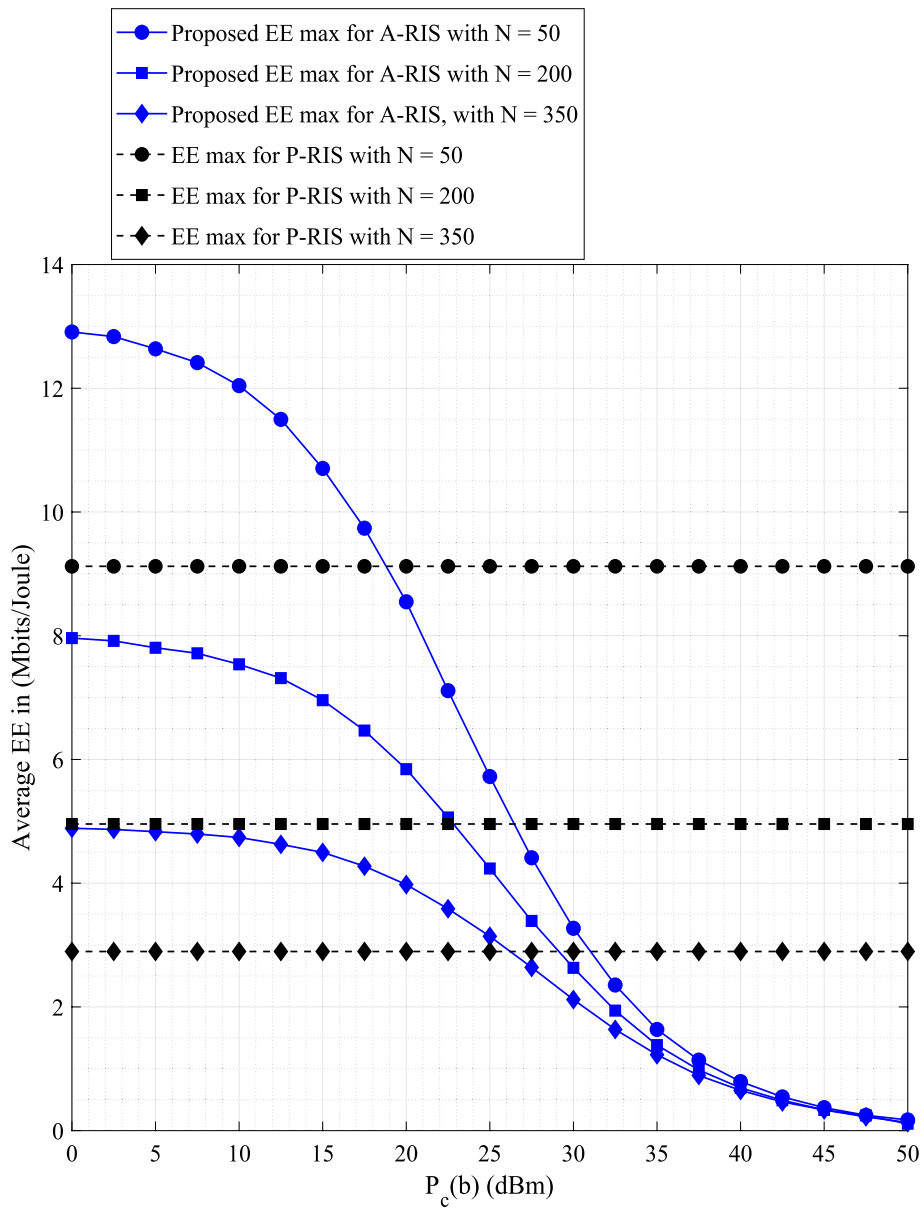
Fig. 5 Average SE versus $P_{\max}$ for $R_{\min} = 0$ bits/Hz with $N = 64$, $P_c(b) = 7.8$mW, $M = 64$, $K = 8$

Figure 7 illustrates the feasibility of the problem with respect to the minimum rate required per user. As expected, the feasibility of the problem decreases with the increase of the minimum required for each user ($R_{\min,k}$).
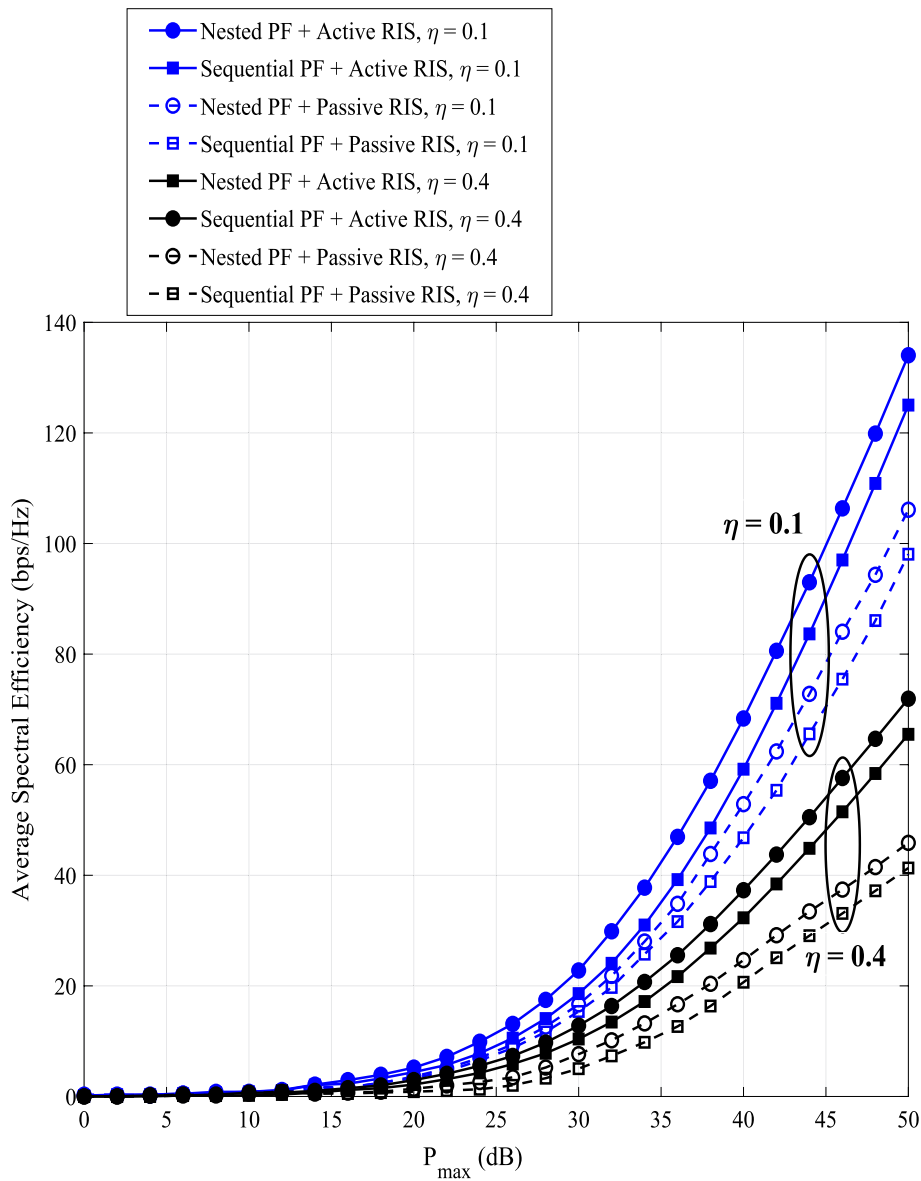
Fig. 6 Average communication EE versus $P_c(b)$ for different number of reflecting elements N, $M = 64$, $K = 8$

5 Conclusion

This study focused on enhancing the communication EE of RIS-based multi-user ISAC systems. Two algorithms based on alternating maximization have been developed for the considered framework. The findings indicate that the proposed active RIS system outperforms passive RIS systems for small number of reflecting elements,
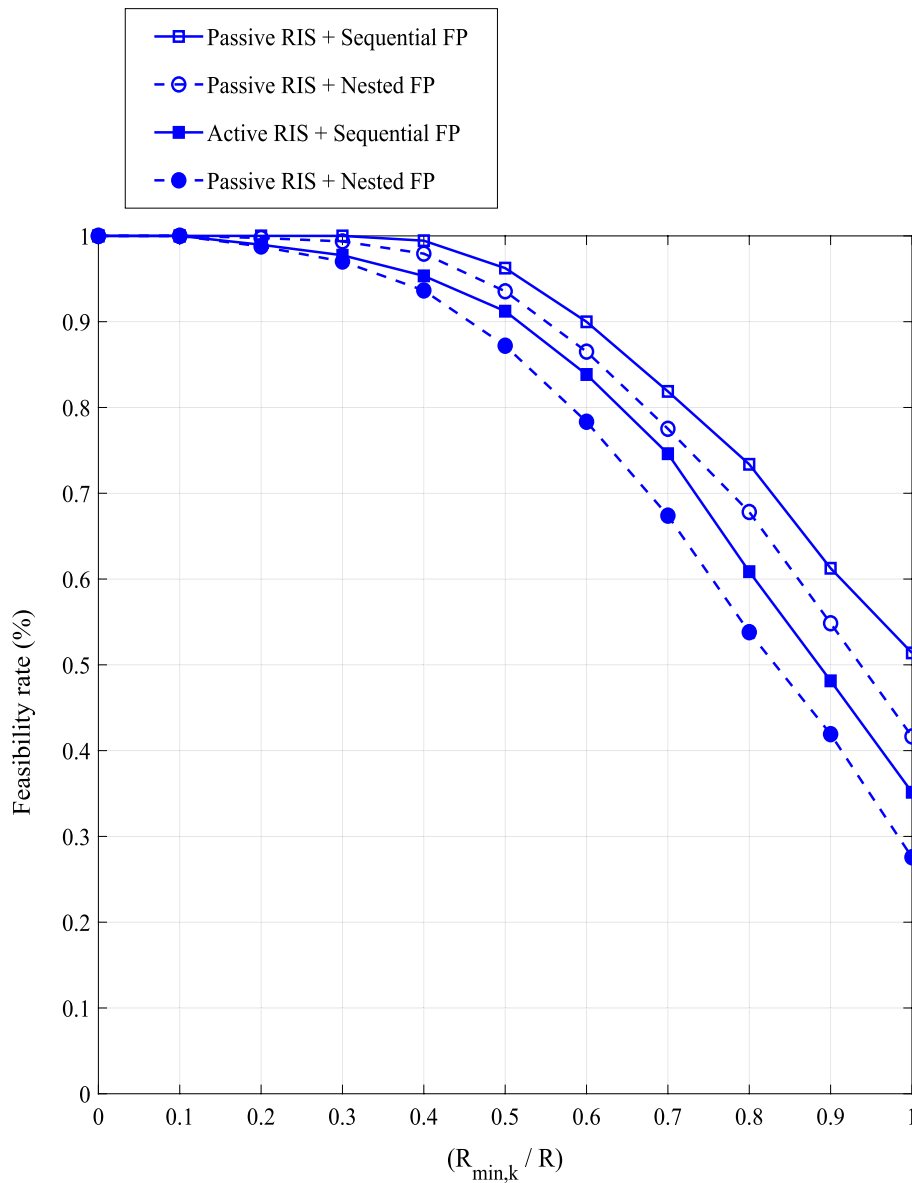
Fig. 7 Feasibility rate versus the fraction of R ($R_{min,k}/R$) at $P_{max} = 25dBW, M = 64, K = 8$

but once the number of elements exceeds a specific number, their consumed power inverts the trend making passive RIS more energy efficient than active counterpart. The impact of the fraction of power allocated for sensing function and the circuit consumed power dissipation of the RIS reflecting elements on the overall EE performance of the ISAC system was investigated.
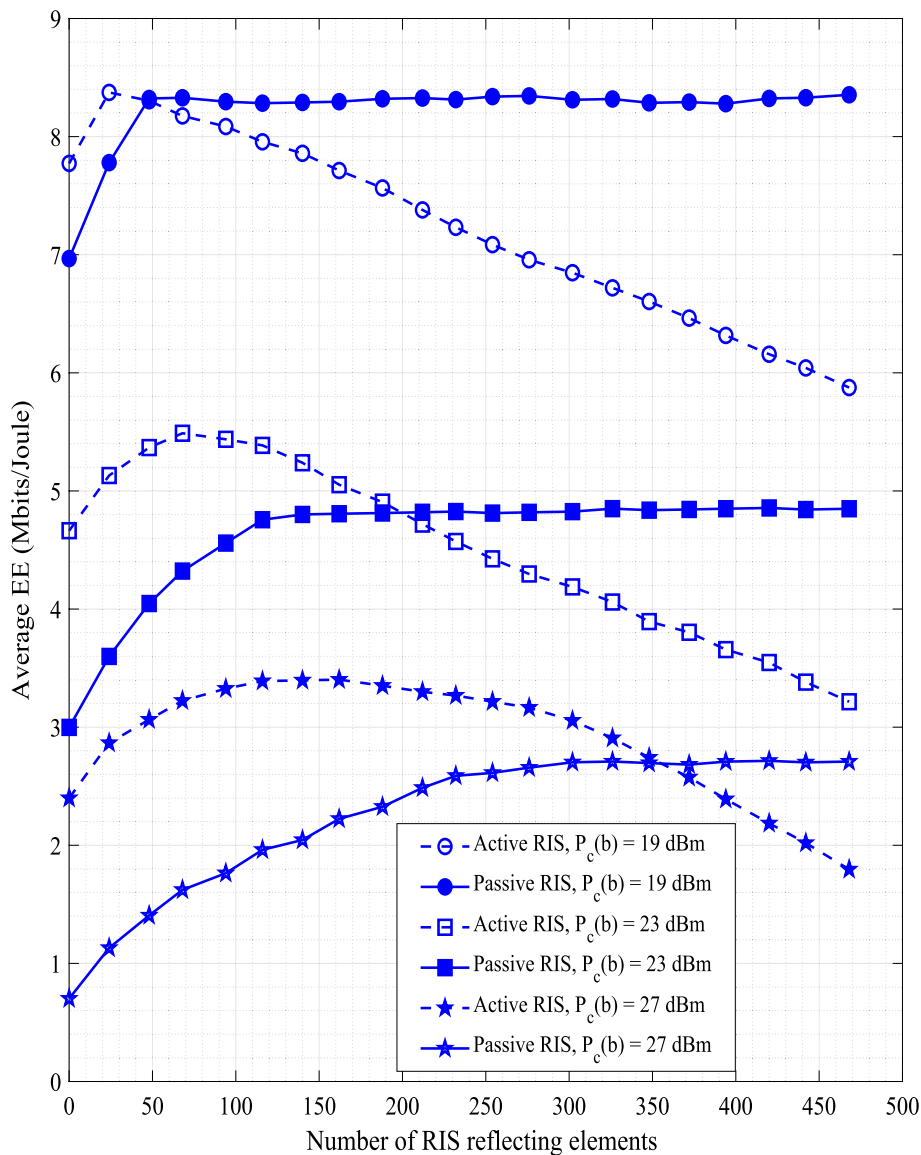
Fig. 8 Average communication EE versus N for different $P_c(b)$ values, with $N = 64$, $P_c(b) = 7.8$mW, $M = 64$, $K = 8$

Author contributions
MR developed the idea, wrote the paper, developed the simulation code, and managed the discussion. AZ helped in mathematical modeling, discussing the results, and polishing thoroughly the paper. SB was involved in discussing the technical idea, polishing the paper, and writing the results section. DW contributed to mathematical modeling, designing the problem, discussing the proposed algorithms. AD helped to manage the discussion, polish the paper thoroughly, and adjust the writing of the paper.

Availability of data and material
My manuscript has no associated data.

Declarations

Competing interests
All authors do not have any financial and non-financial conflict of interest.

References

1. S. Buzzi, I. Chih-Lin, T.E. Klein, H.V. Poor, C. Yang, A. Zappone, A survey of energy-efficient techniques for 5G networks and challenges ahead. IEEE J. Sel. Areas Commun. **34**(4), 697–709 (2016)
2. S. Buzzi, C. D'Andrea, M. Lops, Using massive MIMO arrays for joint communication and sensing. in *53rd IEEE Asilomar Conference*, pp. 5–9. IEEE (2019)
3. L.N. Ribeiro, S. Schwarz, M. Rupp, A.L.F. Almeida, Energy efficiency of mmWave massive MIMO precoding with low-resolution DACs. IEEE J. Sel. Topics Signal Process. **12**(2), 298–312 (2018)
4. C. Huang, A. Zappone, G.C. Alexandropoulos, M. Debbah, C. Yuen, Reconfigurable intelligent surfaces for energy efficiency in wireless communication. IEEE Trans. Wirel. Commun. **18**(8), 4157–4170 (2019)
5. Z. Yang, M. Chen, W. Saad, W. Xu, M. Shikh-Bahaei, H.V. Poor, S. Cui, Energy-efficient wireless communications with distributed reconfigurable intelligent surfaces. IEEE Trans. Wirel. Commun. **21**(1), 665–679 (2022)
6. F. Liu, Y. Cui, C. Masouros, J. Xu, T.X. Han, Y.C. Eldar, S. Buzzi, Integrated sensing and communications: toward dual-functional wireless networks for 6G and beyond. IEEE J. Sel. Areas Commun. **40**(6), 1728–1767 (2022)
7. M. Di Renzo, A. Zappone, M. Debbah, M.-S. Alouini, C. Yuen, J. De Rosny, S. Tretyakov, Smart radio environments empowered by reconfigurable intelligent surfaces: how it works, state of research, and the road ahead. IEEE J. Sel. Areas Commun. **38**(11), 2450–2525 (2020)
8. Z. Lin, M. Lin, B. Champagne, W.-P. Zhu, N. Al-Dhahir, Secrecy-energy efficient hybrid beamforming for satellite-terrestrial integrated networks. IEEE Trans. Commun. **69**(9), 6345–6360 (2021). https://doi.org/10.1109/TCOMM.2021.3088898
9. Z. Lin, K. An, H. Niu, Y. Hu, S. Chatzinotas, G. Zheng, J. Wang, Slnr-based secure energy efficient beamforming in multibeam satellite systems. IEEE Trans. Aerosp. Electron. Syst. **59**(2), 2085–2088 (2023). https://doi.org/10.1109/TAES.2022.3190238
10. M. Rihan, E. Grossi, L. Venturino, S. Buzzi, Spatial diversity in radar detection via active reconfigurable intelligent surfaces. IEEE Signal Process. Lett. **29**, 1242–1246 (2022)
11. S. Buzzi, E. Grossi, M. Lops, L. Venturino, Foundations of MIMO radar detection aided by reconfigurable intelligent surfaces. IEEE Trans. Signal Process. **70**, 1749–1763 (2022)
12. Z.-M. Jiang, M. Rihan, P. Zhang, L. Huang, Q. Deng, J. Zhang, E.M. Mohamed, Intelligent reflecting surface aided dual-function radar and communication system. IEEE Syst. J. **16**(1), 475–486 (2022). https://doi.org/10.1109/JSYST.2021.3057400
13. C. Huang, A. Zappone, G.C. Alexandropoulos, M. Debbah, C. Yuen, Reconfigurable intelligent surfaces for energy efficiency in wireless communication. IEEE Trans. Wirel. Commun. **18**(8), 4157–4170 (2019)
14. H. Shen, W. Xu, S. Gong, Z. He, C. Zhao, Secrecy rate maximization for intelligent reflecting surface assisted multi-antenna communications. IEEE Commun. Lett. **23**(9), 1488–1492 (2019)
15. X. Yu, D. Xu, Y. Sun, D.W.K. Ng, R. Schober, Robust and secure wireless communications via intelligent reflecting surfaces. IEEE J. Sel. Areas Commun. **38**(11), 2637–2652 (2020)
16. M. Rihan, A. Zappone, S. Buzzi, G. Fodor, M. Debbah, Passive vs. active reconfigurable intelligent surfaces for integrated sensing and communication: challenges and opportunities. IEEE Netw. (2023). https://doi.org/10.1109/MNET.2023.3321542
17. M. Rihan, A. Zappone, S. Buzzi, Robust ris-assisted mimo communication-radar coexistence: joint beamforming and waveform design. IEEE Trans. Commun. **71**(11), 6647–6661 (2023). https://doi.org/10.1109/TCOMM.2023.3298983
18. K. Guo, R. Liu, X. Li, L. Yang, K. An, Y. Huang, Outage performance of ris-assisted cognitive non-terrestrial network with noma. IEEE Trans. Veh. Technol. **1**, 5 (2023). https://doi.org/10.1109/TVT.2023.3330329
19. R. Liu, K. Guo, K. An, Y. Huang, F. Zhou, S. Zhu, Resource allocation for cognitive satellite-hap-terrestrial networks with non-orthogonal multiple access. IEEE Trans. Veh. Technol. **72**(7), 9659–9663 (2023). https://doi.org/10.1109/TVT.2023.3252642
20. Z. Lin, H. Niu, K. An, Y. Wang, G. Zheng, S. Chatzinotas, Y. Hu, Refracting ris-aided hybrid satellite-terrestrial relay networks: joint beamforming design and optimization. IEEE Trans. Aerosp. Electron. Syst. **58**(4), 3717–3724 (2022). https://doi.org/10.1109/TAES.2022.3155711
21. Z. Lin, H. Niu, K. An, Y. Hu, D. Li, J. Wang, N. Al-Dhahir, Pain without gain: destructive beamforming from a malicious ris perspective in iot networks. IEEE Internet Things J. **11**(5), 7619–7629 (2024). https://doi.org/10.1109/JIOT.2023.3316830
22. M. Zhu, K. Guo, Y. Ye, L. Yang, T.A. Tsiftsis, H. Liu, Active ris-aided covert communications for miso-noma systems, in *IEEE Wirel. Commun. Lett.* (2023), pp.2203–2207. https://doi.org/10.1109/LWC.2023.3314625

23. S.M. Hamedoon, J.N. Chattha, M. Bilal, Towards intelligent user clustering techniques for non-orthogonal multiple access: a survey. J. Wirel. Comput. Netw. (2024). https://doi.org/10.1186/s13638-024-02333-z

24. K. Guo, M. Wu, X. Li, H. Song, N. Kumar, Deep reinforcement learning and noma-based multi-objective ris-assisted is-uav-tns: trajectory optimization and beamforming design. IEEE Trans. Intell. Transp. Syst. **24**(9), 10197–10210 (2023). https://doi.org/10.1109/TITS.2023.3267607

25. K. Guo, K. An, On the performance of ris-assisted integrated satellite-uav-terrestrial networks with hardware impairments and interference. IEEE Wirel. Commun. Lett. **11**(1), 131–135 (2022). https://doi.org/10.1109/LWC.2021.3122189

26. R. Liu, M. Li, Y. Liu, Q. Wu, Q. Liu, Joint transmit waveform and passive beamforming design for RIS-aided DFRC systems. IEEE J. Sel. Topics Signal Process. **16**(5), 995–1010 (2022)

27. R. Long, Y.-C. Liang, Y. Pei, E.G. Larsson, Active reconfigurable intelligent surface-aided wireless communications. IEEE Trans. Wirel. Commun. **20**(8), 4962–4975 (2021)

28. K. Zhi, C. Pan, H. Ren, K.K. Chai, M. Elkashlan, Active ris versus passive ris: which is superior with the same power budget? IEEE Commun. Lett. **26**(5), 1150–1154 (2022). https://doi.org/10.1109/LCOMM.2022.3159525

29. M. Rihan, A. Zappone, S. Buzzi, G. Fodor, M. Debbah, Passive vs. active reconfigurable intelligent surfaces for integrated sensing and communication: challenges and opportunities. IEEE Netw. (2023) https://doi.org/10.1109/MNET.2023.3321542

30. M. Najafi, V. Jamali, R. Schober, H.V. Poor, Physics-based modeling and scalable optimization of large intelligent reflecting surfaces. IEEE Trans. Commun. **69**(4), 2673–2691 (2021)

31. Z. Zhang, L. Dai, X. Chen, C. Liu, F. Yang, R. Schober, H. Vincent, Poor, active RIS vs passive RIS: which will prevail in 6G? IEEE Trans. Commun. (2022). https://doi.org/10.1109/TCOMM.2022.3231893

32. X. Yue, M. Song, C. Ouyang, Y. Liu, T. Li, T. Hou, Exploiting active ris in noma networks with hardware impairments. IEEE Trans. Veh. Technol. (2024). https://doi.org/10.1109/TVT.2024.3352813

33. G. Lee, H. Lee, J. Oh, J. Chung, J. Choi, Channel estimation for reconfigurable intelligent surface with a few active elements. IEEE Trans. Veh. Technol. **72**(6), 8170–8174 (2023). https://doi.org/10.1109/TVT.2023.3241928

34. G. Zhou, C. Pan, H. Ren, P. Popovski, A.L. Swindlehurst, Channel estimation for ris-aided multiuser millimeter-wave systems. IEEE Trans. Signal Process. **70**, 1478–1492 (2022). https://doi.org/10.1109/TSP.2022.3158024

35. H. Zhang, B. Di, L. Song, Z. Han, Reconfigurable intelligent surfaces assisted communications with limited phase shifts: how many phase shifts are enough? IEEE Trans. Veh. Technol. **69**(4), 4498–4502 (2020). https://doi.org/10.1109/TVT.2020.2973073

36. I. Csiszar, G. Tusnady, Information geometry and alternating minimization procedures. Stat. Decis. **1**, 205–237 (1984)

37. K. Shen, W. Yu, Fractional programming for communication systems-part I: power control and beamforming. IEEE Trans. Signal Process. **66**(10), 2616–2630 (2018)

38. B.R. Marks, G.P. Wright, A general inner approximation algorithm for non-convex mathematical programs. Oper. Res. **26**(4), 681–683 (1978)

39. E. Björnson, L. Sanguinetti, J. Hoydis, M. Debbah, Optimal design of energy-efficient multi-user MIMO systems: is massive MIMO the answer? IEEE Trans. Wirel. Commun. **14**(6), 3059–3075 (2015)

40. Q. Wu, R. Zhang, Intelligent reflecting surface enhanced wireless network via joint active and passive beamforming. IEEE Trans. Wirel. Commun. **18**(11), 5394–5409 (2019). https://doi.org/10.1109/TWC.2019.2936025

Publisher's Note

Springer Nature remains neutral with regard to jurisdictional claims in published maps and institutional affiliations.